How to cite: *Angew. Chem. Int. Ed.* **2022,** *61,* e202202397
International Edition: doi.org/10.1002/anie.202202397
German Edition: doi.org/10.1002/ange.202202397

Luminescent Materials

Transfer of Axial Chirality to the Nanoscale Endows Carbon Nanodots with Circularly Polarized Luminescence

Simone Di Noja, Francesco Amato, Francesco Zinna, Lorenzo Di Bari, Giulio Ragazzon,* and Maurizio Prato**

Dedicated to Prof. Sir. J. Fraser Stoddart on the occasion of his 80th birthday

Abstract: We report the synthesis, purification and characterization of chiral carbon nanodots starting from atropoisomeric precursors. The obtained atropoisomeric carbon nanodots are soluble in organic solvents and have good thermal stability, which are desirable features for technological applications. The synthetic protocol is robust, as it supports a number of variations in terms of molecular doping agents. Remarkably, the combination of axially chiral precursors and 1,4-benzoquinone as doping agent results in green-emissive carbon dots displaying circularly polarized luminescence. Dissymmetry factors of $|3.5| \times 10^{-4}$ are obtained in solution, without the need of any additional element of chirality. Introducing axial chirality expands the strategies available to tailor the properties of carbon nanodots, paving the way for carbon nanoparticles that combine good processability in organic solvents with engineered advanced chiroptical properties.

[*] S. Di Noja, Dr. F. Amato, Dr. G. Ragazzon, Prof. M. Prato
Department of Chemical and Pharmaceutical Sciences, CENMAT, Center of Excellence for Nanostructured Materials, INSTM UdR Trieste,
University of Trieste
via Licio Giorgieri 1, 34127 Trieste (Italy)
E-mail: ragazzon@unistra.fr
prato@units.it

Dr. F. Zinna, Prof. L. Di Bari
Department of Chemistry and Industrial Chemistry
University of Pisa
via Moruzzi 13, 56124 Pisa (Italy)
E-mail: lorenzo.dibari@unipi.it

Dr. G. Ragazzon
CNRS, Institut de Science et d'Ingégnierie Supramoléculaires (ISIS)
University of Strasbourg
8 allée Gaspard Monge, 67000 Strasbourg (France)

Prof. M. Prato
Center for Cooperative Research in Biomaterials (CIC biomaGUNE), Basque Research and Technology Alliance (BRTA)
Paseo de Miramón 182, 20014 Donostia San Sebastián (Spain)
and
Basque Fdn Sci, Ikerbasque 48013 Bilbao (Spain)

Introduction

Carbon nanodots (CNDs) are carbon-based nanoparticles of size up to 10 nm.[1–4] One of the reasons why CNDs received considerable attention from the scientific community is their luminescence, which has been the focus of numerous studies.[5,6] In most cases, desirable luminescent properties are combined with water solubility, facilitating their use in biological applications.[7–9] However, while much less explored, CNDs soluble in non-polar organic solvents are highly desirable for technological applications, e.g. in optoelectronic devices.[10] To date, the few non-polar CNDs reported have been usually obtained via a hot-injection method.[11,12] This methods is reminiscent of the synthesis of inorganic quantum dots, requiring high temperature and inert atmosphere, and so far proved less versatile than the consolidated bottom-up strategies employed in the synthesis of hydrophilic CNDs.[13]

The underdevelopment of non-polar CNDs in comparison with their water soluble analogues is evident also from the lack of chiral non-polar CNDs.[14–17] On this basis, we approached the preparation of chiral and non-polar CNDs leveraging the solvothermal treatment of small molecular precursors.[4,18,19] Indeed, the appropriate selection of starting materials, doping agents, and synthetic conditions affords CNDs with tailored structural and optical properties.[5,20–23] Expanding the solvothermal strategies to non-polar solvents would be desirable, because it can significantly increase the pool of molecular dopants that can be employed, leading to engineered advanced functionalities. In particular, it could facilitate the development of CNDs exhibiting circularly polarized luminescence (CPL), without the need for a chiral matrix. Indeed, to date all the studies reporting CPL from CNDs employed chiral matrices,[24] known to impart CPL even to achiral molecular fluorophores, as opposite to controlling the nanoparticle chirality directly.[25–29]

To achieve CPL, we reasoned that a promising and different strategy would be to employ atropoisomeric precursors. Atropoisomers are molecules that are chiral by virtue of restricted rotation around a single bond, i.e., they are axially chiral.[30–32] Such precursors have not been previously employed for the preparation of CNDs, possibly due to their non-polar nature. However, atropoisomeric units such as binaphthyls are frequently employed as CPL emitters and have high thermal racemization barriers, which

are desirable features to achieve CNDs that display CPL.[33,34] Herein, we report the synthesis and the properties of novel non-polar chiral CNDs derived from atropoisomeric precursors, resulting in CNDs that display intrinsic CPL, good processability in organic solvents, and prolonged thermal stability.

Results and Discussion

To realize atropoisomeric CNDs, we employed citric acid in combination with either (*S*)-1,1′-binaphtyl-2,2′-diamine or its (*R*)-atropoisomer. Citric acid was selected for its consolidated ability to afford CNDs under several synthetic conditions.[35,36] Binaphthyl diamines were chosen because diamines are frequently used as doping agents in CND synthesis, and the naphthyl groups could impart hydrophobicity to the resulting CNDs.[37] Moreover, these axially chiral precursors have high thermal stability, with a lifetime of 23 h at 250 °C.[38] Using *N,N*-dimethylformamide (DMF) as the solvent was critical for the success of our synthetic procedure, because DMF can solubilize the atropoisomeric diamine, allowing it to react. This combination of reactants and solvent afforded chiral nanoparticles, termed **CNDs-1**. (Scheme 1, top reaction arrow) Indeed, atomic force microscopy (AFM) experiments revealed particles having a size of 3.5 nm, and electronic circular dichroism (ECD) of **CNDs-*S*-1** and **CNDs-*R*-1** displayed mirror-image spectra having a maximum at 287 nm (see Supporting Information Figure S5b). **CNDs-1** emit in the blue region of the spectrum, with a maximum emission intensity at 387 nm (see Supporting Information Figure S5c–d).

In order to improve the optical properties of atropoisomeric CNDs, shifting the emission in the green region of the visible spectrum, we explored the use of doping agents. Upon screening of several carbonyl compounds (see Supporting Information Table S1 and Figure S7), we selected 1,4-benzoquinone as a suitable doping agent because it can participate in CNDs formation and can react with aromatic amines as Michael acceptor at both position 2 and 5, promoting the formation of extended conjugated polymer structure.[39,40] Thus, (*S*)- or (*R*)- atropoisomeric 1,1′-binaphthyl-2,2′-diamine, citric acid and an optimized amount of benzoquinone were mixed in DMF and heated up to 240 °C in a microwave reactor (see Scheme 1, bottom reaction arrow, Supporting Information Experimental Procedure, Table S2 and Figure S8). Simple mixing of benzoquinone with the other precursors afforded a burgundy color mixture, this color change was not observed for **CNDs-1**, indicating that 1,4-benzoquinone reacts with atropoisomeric amines already at room temperature. The mixture turned into a dark brown solution upon microwave treatment. The crude was filtered to remove any large particle, and **CNDs-2** were precipitated from diethyl ether. The effective removal of small molecules using this straightforward purification procedure was confirmed by thin-layer chromatography analysis and ^{1}H NMR. Further validation of the purification procedure was obtained performing an additional size-exclusion chromatographic separation, which afforded fractions having similar optical properties, indicating material homogeneity (see Supporting Information Figure S9).[41,42] The obtained CNDs, termed **CNDs-*S*-2** or **CNDs-*R*-2**, are soluble (e.g. $>20\,mg\,mL^{-1}$) in common polar organic solvents, such as DMF, DMSO, chloroform, and dichloromethane, indicating good processability. Partial solubility in water can also be achieved (see Supporting Information, Experimental Procedure).

Structural and morphological information on atropoisomeric **CNDs-2** was obtained by transmission electron microscopy (TEM), AFM, X-ray photoelectron spectroscopy (XPS), Fourier-transform infrared spectroscopy (FT-IR), and nuclear magnetic resonance (NMR) analysis. TEM analysis of **CNDs-*S*-2** reveals particles having a mean size of 3.5 nm (Figure 1a and Figure S10). The quasi-spherical nature of **CNDs-*S*-2** was confirmed by AFM analysis, which showed a uniform height distribution centered at 3.58 ± 0.55 nm, fully consistent with the TEM data (Figure 1b,c and Figure S11). XPS analysis for **CNDs-*S*-2** indicates effective nitrogen inclusion into the nanomaterial, with 5.7 % N, 14.2 % O, and 79.5 % C observed. Deconvolution of C1s peak indicates that ca. 50 % of C participate in C=C bonds and reveals the presence of residual COOH groups. Analysis of N1s peak indicates amino groups as the main component, with an increase in C=N bonds observed upon benzoquinone addition, i.e., in comparison with **CNDs-1** (see Supporting Information Figure S12–S15 and Table S3, S4). Coherent information is obtained from FTIR by comparison with the starting materials (Figure S16–S19). The two sharp N–H stretching signals of the diamine precursor at 3475 and 3382 cm^{-1} disappeared, with new signals observed between 1618 and 1573 cm^{-1}, in the region of N–H bending.

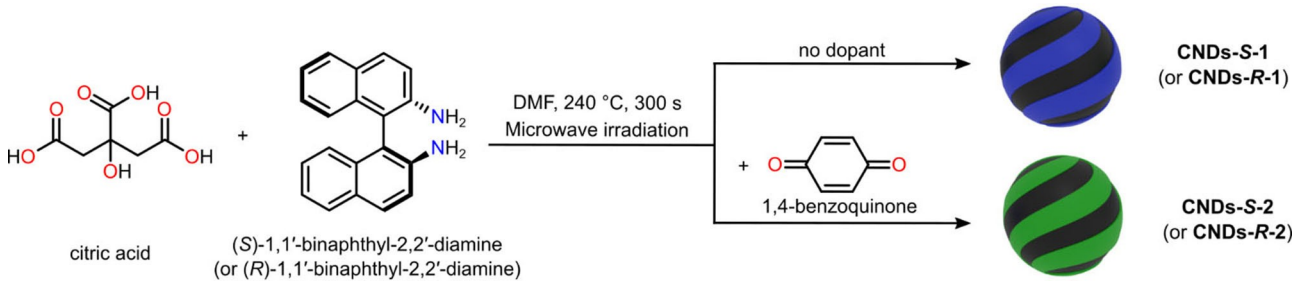

Scheme 1. Synthesis of atropoisomeric CNDs.

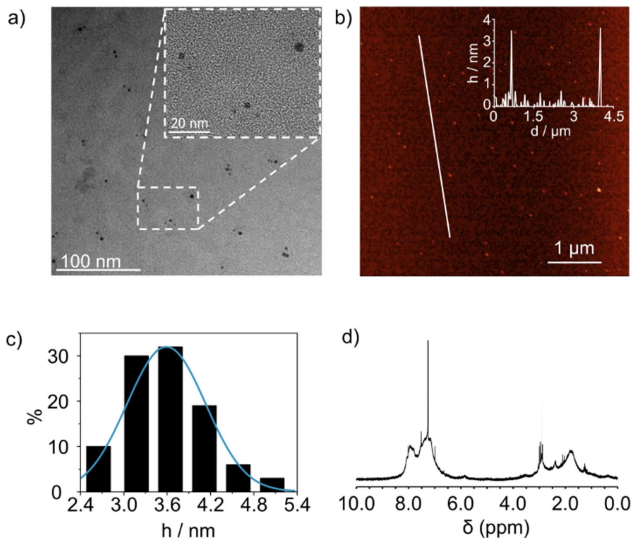

Figure 1. Morphological characterization of **CNDs-2**. (a) TEM image of **CNDs-*S*-2**: inset is the dashed area at higher magnification. b) Tapping mode AFM of **CNDs-*S*-2** deposited on a mica substrate; inset is the height profile along the white solid line. c) Size histogram of AFM height data, with distribution fit (blue curve) based on a Gaussian distribution. Statistical analysis is carried out on 100 nanoparticles. d) ^{1}H NMR ($CDCl_3$, 400 MHz, r.t.) of **CNDs-*S*-2**.

The presence of binaphthyl units is confirmed by the distinctive strong signals at 815 and 749 cm^{-1}, assigned to the out-of-plane bending of aromatic C–H bonds, which are slightly shifted with respect to the starting diamine.[43] The presence of carbonyl functional groups is indicated by an intense signal at 1707 cm^{-1}, which originates mainly from citric acid, as revealed by the comparison with **CNDs-1**, obtained in the absence of benzoquinone, which nevertheless show a similar peak at 1709 cm^{-1} (Figure S19). ^{1}H NMR of **CNDs-*S*-2** (Figure 1d) displays broad signals in the aromatic (8.5–6.5 ppm) and aliphatic (3.5–1 ppm) regions of the spectrum, together with a less intense broad signal at ca. 6 ppm, pointing at the inclusion of all precursors. Broad signals are coherent with the formation of particles, leading to H atoms experiencing different environments and slow rotation.[44] Analogous results are observed for **CNDs-*R*-2** (see Supporting Information Figure S20).

The UV-vis absorption spectra of **CNDs-*S*-2** and **CNDs-*R*-2** in $CHCl_3$ (Figure 2a) display broad absorption bands extending into the visible region up to 600 nm. Non-structured shoulders appear at 285 and 425 nm. Since none of the precursors absorbs above 400 nm, **CNDs-2** formation affords low-energy optical transitions in the visible region. On the basis of color changes observed upon mixing the precursors, we tentatively ascribe the new band to an extended conjugation of the atropoisomeric moiety. The ECD spectra of **CNDs-*S*-2** and **CNDs-*R*-2** in $CHCl_3$ (Figure 2b) demonstrate the chiral nature of atropoisomeric **CNDs-2**. Indeed, the two spectra have equal intensity and opposite sign. The ECD spectrum displays the low-energy transition in the visible characteristic of atropoisomeric **CNDs-2**. This new band, centered around 417 nm, is

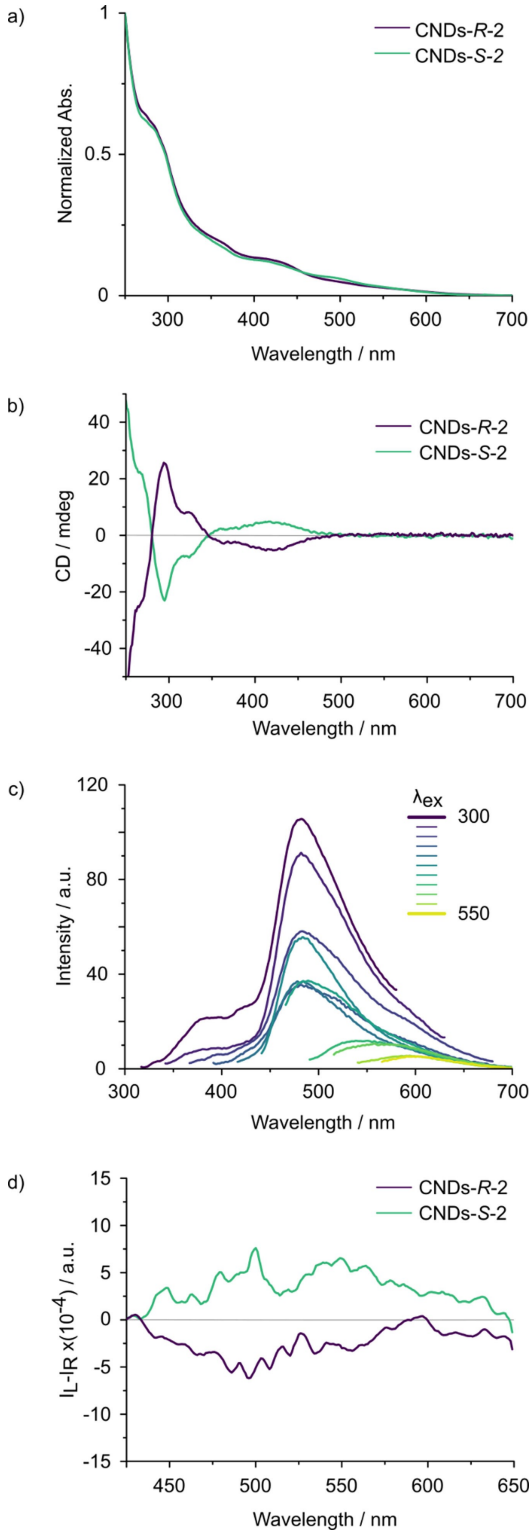

Figure 2. Photophysical characterization of **CNDs-*R*-2** and **CNDs-*S*-2**. a) UV-vis spectra of **CNDs-*R*-2** (violet line) and **CNDs-*S*-2** (green line) in $CHCl_3$. b) ECD spectra of **CNDs-*R*-2** (violet line) and **CNDs-*S*-2** (green line) in $CHCl_3$. c) Fluorescence emission spectra of **CNDs-*S*-2** recorded at different excitation wavelengths in $CHCl_3$. d) CPL spectra of **CNDs-*R*-2** (violet line) and **CNDs-*S*-2** (green line) in CH_2Cl_2, excited at 365 nm. Experiments were performed at r.t., at concentrations between 0.01 and 0.05 mg mL^{-1}.

associated with an absorption dissymmetry factor (g_{abs}) of $|4.6| \times 10^{-4}$, which increases up to $|6.0| \times 10^{-4}$, in highly polar organic solvents such as DMF or Ethanol (Table S5 and Figure S21). For comparison, in the starting diamine the most red-shifted ECD band (336 nm) was associated to a g_{abs} of ($|2.6| \times 10^{-3}$). Thus, axial chirality is effectively transferred to the nanomaterial. Moreover, a survey of synthesis temperature and time suggests that temperature-induced racemization is not relevant up to 240 °C, and reveals that longer reaction times afford higher g_{abs} values (see Supporting Information Table S2). The emission spectra of **CND-*S*-2** show a main emission band in the green region, peaking at 480 nm and displaying an excitation wavelength-dependent profile (Figure 2c and Figure S22). Since the starting diamine emits in the blue region, with an emission centered at 400 nm (see Supporting Information Figure S19), **CNDs-*S*-2** formation leads to a significant bathochromic shift of the emission (80 nm). We investigated the emission properties in multiple solvents (Table S5 and Figure S21), observing no significant variation of the emission wavelength upon changing solvent, which supports the idea of an extended conjugation as origin of the bathochromic shift, rather than a charge-transfer effect. Less intense emissions extending up to 650 nm are also observed, typical of CNDs. Accordingly, the luminescence quantum yield changes with the excitation wavelength, with a value of 0.4 % at 450 nm for **CNDs-*S*-2**, in correspondence of the lowest-energy chiral absorption band. Similar results were observed for atropoisomeric **CNDs-*R*-2** (see Supporting Information Figure S24).

Remarkably, upon 365 nm irradiation, **CNDs-2** samples displayed opposite CPL bands centered around 500 nm (negative for **CNDs-*R*-2** and positive for **CNDs-*S*-2**, which retrace the luminescence profile (Figure 2d). Luminescence dissymmetry factors (g_{lum}) are fairly constant throughout the emission region. Average g_{lum} values were estimated as the ratio between the integral of CPL and the integral of total intensity spectrum calculated in the 420–640 nm range, providing $g_{lum} = +3.6 \times 10^{-4}$ and -3.4×10^{-4} for **CNDs-*S*-2** and **CNDs-*R*-2**, respectively (see Supporting Information Figure S25). Such values are in line with the respective absorption dissymmetry factor g_{abs} of the most red-shifted Cotton effect in the ECD spectra (417 nm, see above). This indicates a similar stereochemistry of the ground and emitting excited state.[34] Similar results were obtained in a more polar solvent such as DMF, where $g_{lum} = +4/-3 \times 10^{-4}$ were measured for **CNDs-*S*-2**/**CNDs-*R*-2**. (Figure S26). To investigate the role of 1,1′-binaphtyl-2,2′-diamine in CPL generation, we have prepared CNDs in its absence. The obtained achiral material emits at a different wavelength (465 nm) with respect to atropoisomeric **CNDs-2** and has a more pronounced excitation-dependent emission, suggesting that the chiral diamine participates directly to the formation of fluorophores responsible of CPL (see Supporting Information Figure S27–28). On the other hand, 1,1′-binaphtyl-2,2′-diamine alone displays CPL activity in the UV/violet region with a maximum around 395 nm and g_{lum} around $-9/+8 \times 10^{-4}$ for *R*- and *S*-enantiomer respectively (see Supporting Information Figure S23, S29).

Thermogravimetric analysis indicates a moderate weight loss up to 350 °C, possibly due to decarboxylation reactions, followed by a significant weight loss above 400 °C, which might be attributed to Csp^3-rich domains (see Figure 3a and Supporting Information Figure S30).[45] A residual 43 % weight at 700 °C for both **CNDs-2** further substantiates the abundance of aromatic structures, in full agreement with XPS analysis. On the basis of the negligible weight loss observed at 100 °C, we tested the thermal stability of **CNDs-2** in time. Even after 150 h at 100 °C under air, the g_{abs} of **CNDs-*S*-2** and **CNDs-*R*-2** remained unchanged. Remarkably, while the g_{lum} values are lower than other nanostructured systems, this is the first case in which thermal stability could be investigated.[46–50] The stability of atropoisomeric **CNDs-2**, combined with their good processability, makes this type of nanoparticles suitable candidates for technological applications of CPL under harsh conditions.

Conclusion

In conclusion, we have successfully shown that axially chiral information can be retained in the synthesis of CNDs, leading to carbon-based nanoparticles displaying CPL as an intrinsic property. Indeed, by preparing novel non-polar

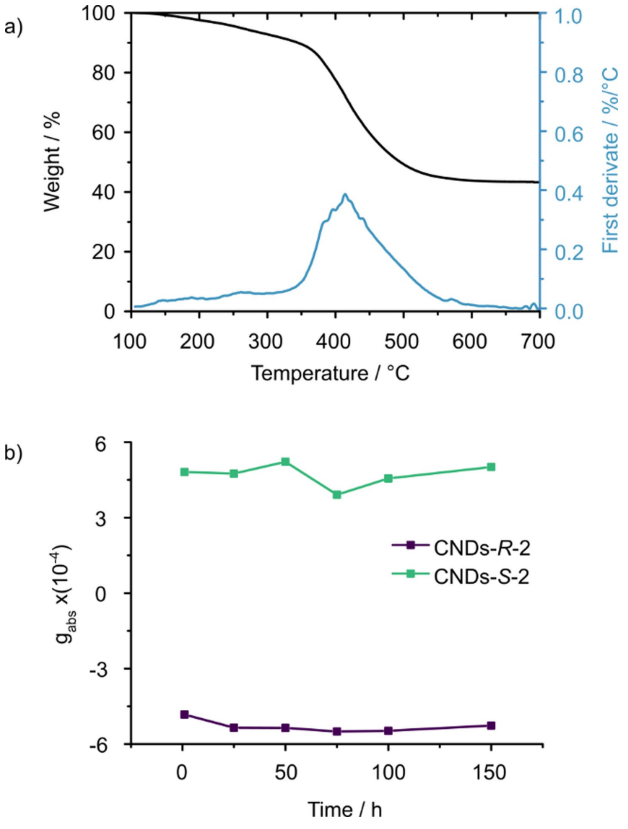

Figure 3. Thermal characterization of **CNDs-2**. a) Thermogravimetric analysis of **CNDs-*S*-2** (black line) and its first derivative (blue line). Analysis performed under nitrogen atmosphere. (b) g_{abs} of **CNDs-*R*-2** (violet squares) and **CNDs-*S*-2** (green squares) after thermal treatment at 100 °C in an oven for the indicated time.

chiral CNDs from atropoisomeric precursors, the axial chirality of the starting material is extended from molecular to nanoscale, resulting in nanomaterials having advanced functionality. Achieving intrinsic CPL from an easily processable and thermally stable nanoparticle demonstrates the potential of engineering nanomaterials at the molecular level.[51]

Acknowledgements

M.P. is the AXA Chair for Bionanotechnology (2016–2023). The authors gratefully acknowledge the financial support from the European Research Council (ERC AdG-2019 n° 885323, e-DOTS), the Spanish Ministerio de Ciencia, Innovación y Universidades (project PID2019-108523RB-I00), the University of Trieste, INSTM, Italian Ministry of Education MIUR (cofin Prot. 2017PBXPN4) and the Maria de Maeztu Units of Excellence Program from the Spanish State Research Agency (Grant No. MDM-2017-0720). The authors thank Dr. Desirè Di Silvio (CIC biomaGUNE) for performing XPS analyses and Dr. Slavko Kralj (Jožef Stefan Institute) for the assistance with TEM microscopy and the CENN Nanocenter (Slovenia) for TEM access. We thank Paolo Bertoncin (University of Trieste) for preliminary TEM experiments, Dr. Giacomo Filippini and Dr. Marina Garrido Serrano for preliminary experiments, and Simone Adorinni for assistance in image preparation. Open Access Funding provided by Universita degli Studi di Trieste within the CRUI-CARE Agreement.

Conflict of Interest

The authors declare no conflict of interest.

Data Availability Statement

The data that support the findings of this study are available in the Supporting Information of this article.

Keywords: Atropoisomers · Carbon Nanodots · Chirality · Circularly Polarized Luminescence · Nanotechnology

[1] S. N. Baker, G. A. Baker, *Angew. Chem. Int. Ed.* **2010**, *49*, 6726–6744; *Angew. Chem.* **2010**, *122*, 6876–6896.
[2] S. Y. Lim, W. Shen, Z. Gao, *Chem. Soc. Rev.* **2015**, *44*, 362–381.
[3] C. Xia, S. Zhu, T. Feng, M. Yang, B. Yang, *Adv. Sci.* **2019**, *6*, 1901316.
[4] Y.-P. Sun, *Carbon Dots*, Springer Nature, Cham, **2020**.
[5] G. Ragazzon, A. Cadranel, E. V. Ushakova, Y. Wang, D. M. Guldi, A. L. Rogach, N. A. Kotov, M. Prato, *Chem* **2021**, *7*, 606–628.
[6] J. Bai, G. Yuan, Y. Zhu, Z. Huang, L. Zhang, X. Wang, S. Wu, L. Ren, *J. Phys. Chem. C* **2021**, *125*, 18543–18551.
[7] K. Hola, Y. Zhang, Y. Wang, E. P. Giannelis, R. Zboril, A. L. Rogach, *Nano Today* **2014**, *9*, 590–603.
[8] F. Yuan, S. Li, Z. Fan, X. Meng, L. Fan, S. Yang, *Nano Today* **2016**, *11*, 565–586.
[9] L. Đorđević, F. Arcudi, M. Cacioppo, M. Prato, *Nat. Nanotechnol.* **2022**, 17, 112–130.
[10] X. Li, M. Rui, J. Song, Z. Shen, H. Zeng, *Adv. Funct. Mater.* **2015**, *25*, 4929–4947.
[11] F. Wang, S. Pang, L. Wang, Q. Li, M. Kreiter, C. Y. Liu, *Chem. Mater.* **2010**, *22*, 4528–4530.
[12] A. Panniello, A. E. Di Mauro, E. Fanizza, N. Depalo, A. Agostiano, M. L. Curri, M. Striccoli, *J. Phys. Chem. C* **2018**, *122*, 839–849.
[13] Y. Choi, Y. Choi, O. H. Kwon, B. S. Kim, *Chem. Asian J.* **2018**, *13*, 586–598.
[14] M. Wu, J. Zhan, B. Geng, P. He, K. Wu, L. Wang, G. Xu, Z. Li, L. Yin, D. Pan, *Nanoscale* **2017**, *9*, 13195–13202.
[15] Q. Wang, Y. Gao, B. Wang, Y. Guo, U. Ahmad, Y. Wang, Y. Wang, S. Lu, H. Li, G. Zhou, *J. Mater. Chem. C* **2020**, *8*, 4343–4349.
[16] G. Minervini, A. Panniello, E. Fanizza, A. Agostiano, M. L. Curri, M. Striccoli, *Materials* **2020**, *13*, 3716.
[17] H. Yang, Y. Liu, Z. Guo, B. Lei, J. Zhuang, X. Zhang, Z. Liu, C. Hu, *Nat. Commun.* **2019**, *10*, 1789.
[18] L. Đorđević, F. Arcudi, M. Prato, *Nat. Protoc.* **2019**, *14*, 2931–2953.
[19] T. V. De Medeiros, J. Manioudakis, F. Noun, J. R. Macairan, F. Victoria, R. Naccache, *J. Mater. Chem. C* **2019**, *7*, 7175–7195.
[20] C. J. Reckmeier, J. Schneider, A. S. Susha, A. L. Rogach, *Opt. Express* **2016**, *24*, A312–A340.
[21] C. Hu, M. Li, J. Qiu, Y. P. Sun, *Chem. Soc. Rev.* **2019**, *48*, 2315–2337.
[22] F. Arcudi, L. Đorđević, M. Prato, *Acc. Chem. Res.* **2019**, *52*, 2070–2079.
[23] L. Đorđević, F. Arcudi, A. D'Urso, M. Cacioppo, N. Micali, T. Bürgi, R. Purrello, M. Prato, *Nat. Commun.* **2018**, *9*, 3442.
[24] T. Goto, Y. Okazaki, M. Ueki, Y. Kuwahara, M. Takafuji, R. Oda, H. Ihara, *Angew. Chem. Int. Ed.* **2017**, *56*, 2989–2993; *Angew. Chem.* **2017**, *129*, 3035–3039.
[25] A. Li, D. Zheng, M. Zhang, B. Wu, L. Zhu, *Langmuir* **2020**, *36*, 8965–8970.
[26] M. Chekini, E. Prince, L. Zhao, H. Mundoor, I. I. Smalyukh, E. Kumacheva, *Adv. Opt. Mater.* **2020**, *8*, 1901911.
[27] Y. Ru, L. Sui, H. Song, X. Liu, Z. Tang, S.-Q. Zang, B. Yang, S. Lu, *Angew. Chem. Int. Ed.* **2021**, *60*, 14091–14099; *Angew. Chem.* **2021**, *133*, 14210–14218.
[28] C. Zou, D. Qu, H. Jiang, D. Lu, X. Ma, Z. Zhao, Y. Xu, *Molecules* **2019**, *24*, 1008.
[29] M. Xu, X. Wu, Y. Yang, C. Ma, W. Li, H. Yu, Z. Chen, J. Li, K. Zhang, S. Liu, *ACS Nano* **2020**, *14*, 11130–11139.
[30] C. Rosini, L. Franzini, A. Raffaelli, P. Salvadori, *Synthesis* **1992**, *6*, 503–517.
[31] G. Bringmann, A. J. P. Mortimer, P. A. Keller, M. J. Gresser, J. Garner, M. Breuning, *Angew. Chem. Int. Ed.* **2005**, *44*, 5384–5427; *Angew. Chem.* **2005**, *117*, 5518–5563.
[32] E. Kumarasamy, R. Raghunathan, M. P. Sibi, J. Sivaguru, *Chem. Rev.* **2015**, *115*, 11239–11300.
[33] Z. Liu, Z. Jiang, C. He, Y. Chen, Z. Guo, *Dyes Pigm.* **2020**, *181*, 108593.
[34] H. Tanaka, Y. Inoue, T. Mori, *ChemPhotoChem* **2018**, *2*, 386–402.
[35] J. Schneider, C. J. Reckmeier, Y. Xiong, M. Von Seckendorff, A. S. Susha, P. Kasak, A. L. Rogach, *J. Phys. Chem. C* **2017**, *121*, 2014–2022.
[36] R. Ludmerczki, S. Mura, C. M. Carbonaro, I. M. Mandity, M. Carraro, N. Senes, S. Garroni, G. Granozzi, L. Calvillo, S. Marras, L. Malfatti, P. Innocenzi, *Chem. Eur. J.* **2019**, *25*, 11963–11974.

[37] A. Shockravi, A. Javadi, E. Abouzari-Lotf, *RSC Adv.* **2013**, *3*, 6717–6746.
[38] D. C. Patel, R. M. Woods, Z. S. Breitbach, A. Berthod, D. W. Armstrong, *Tetrahedron: Asymmetry* **2017**, *28*, 1557–1561.
[39] F. Rigodanza, L. Đorđević, F. Arcudi, M. Prato, *Angew. Chem. Int. Ed.* **2018**, *57*, 5062–5067; *Angew. Chem.* **2018**, *130*, 5156–5161.
[40] J. Stejskal, P. Bober, M. Trchová, J. Horský, J. Pilař, Z. Walterová, *Synth. Met.* **2014**, *192*, 66–73.
[41] F. Arcudi, L. Đorđević, M. Prato, *Angew. Chem. Int. Ed.* **2016**, *55*, 2107–2112; *Angew. Chem.* **2016**, *128*, 2147–2152.
[42] J. B. Essner, J. A. Kist, L. Polo-Parada, G. A. Baker, *Chem. Mater.* **2018**, *30*, 1878–1887.
[43] Z. Zhang, W. Wang, S. Liu, D. Chen, *Chin. J. Chem. Phys.* **2017**, *30*, 7–15.
[44] B. Bartolomei, A. Bogo, F. Amato, G. Ragazzon, M. Prato, *Angew. Chem. Int. Ed.* **2022**, *61*, e202200038; *Angew. Chem.* **2022**, *134*, e202200038.
[45] "*Thermogravimetric Analysis of Polymers*": H. M. Ng, N. M. Saidi, F. S. Omar, K. Ramesh, S. Ramesh, S. Bashir, *Encyclopedia of Polymer Science and Technology*, Wiley, Hoboken, **2018**, pp. 1–29.
[46] M. Naito, K. Iwahori, A. Miura, M. Yamane, I. Yamashita, *Angew. Chem. Int. Ed.* **2010**, *49*, 7006–7009; *Angew. Chem.* **2010**, *122*, 7160–7163.
[47] U. Tohgha, K. K. Deol, A. G. Porter, S. G. Bartko, J. K. Choi, B. M. Leonard, K. Varga, J. Kubelka, G. Muller, M. Balaz, *ACS Nano* **2013**, *7*, 11094–11102.
[48] Y. Shi, P. Duan, S. Huo, Y. Li, M. Liu, *Adv. Mater.* **2018**, *30*, 1705011.
[49] Y. Sang, J. Han, T. Zhao, P. Duan, M. Liu, *Adv. Mater.* **2020**, *32*, 1900110.
[50] M. Zhang, K. Li, S. Zang, *Adv. Opt. Mater.* **2020**, *8*, 1902152.
[51] M. C. Roco, *AIChE J.* **2004**, *50*, 890–897.

Manuscript received: February 13, 2022
Accepted manuscript online: April 13, 2022
Version of record online: May 5, 2022